




Article

A Comprehensive Study of Al_{0.6}Ti_{0.4}N Coatings Deposited by Cathodic Arc and HiPIMS PVD Methods in Relation to Their Cutting Performance during the Machining of an Inconel 718 Alloy

Luca W. Reolon ¹, Myriam H. Aguirre ^{2,3}, Kenji Yamamoto ⁴, Qinfu Zhao ⁵, Igor Zhitomirsky ⁵, German Fox-Rabinovich ^{1,*} and Stephen Clarence Veldhuis ¹

¹ Department of Mechanical Engineering, McMaster Manufacturing Research Institute (MMRI), McMaster University, 1280 Main Street West, Hamilton, ON L8S 4L7, Canada; reolonl@mcmaster.ca (L.W.R.); veldhu@mcmaster.ca (S.C.V.)

² LMA-Laboratory of Advanced Microscopy, INA—Institute of Nanoscience of Aragón, University of Zaragoza, E-50018 Zaragoza, Spain; maguirre@unizar.es

³ Department of Physics Condensed Matter, University of Zaragoza, E-50009 Zaragoza, Spain

⁴ Applied Physics Research Laboratory, Kobe Steel Ltd., 1-5-5 Takatsuda-dai, Nishi-ku, Kobe, Hyogo 651-2271, Japan; yamamoto.kenji1@kobelco.com

⁵ Department of Material Science and Engineering, McMaster University, 1280 Main Street West, Hamilton, ON L8S 4L7, Canada; zhaoq36@mcmaster.ca (Q.Z.); zhitom@mcmaster.ca (I.Z.)

* Correspondence: gfox@mcmaster.ca



Citation: Reolon, L.W.; Aguirre, M.H.; Yamamoto, K.; Zhao, Q.; Zhitomirsky, I.; Fox-Rabinovich, G.; Veldhuis, S.C. A Comprehensive Study of Al_{0.6}Ti_{0.4}N Coatings Deposited by Cathodic Arc and HiPIMS PVD Methods in Relation to Their Cutting Performance during the Machining of an Inconel 718 Alloy. *Coatings* **2021**, *11*, 723. <https://doi.org/10.3390/coatings11060723>

Academic Editor: Mingwen Bai

Received: 26 May 2021

Accepted: 12 June 2021

Published: 16 June 2021

Publisher's Note: MDPI stays neutral with regard to jurisdictional claims in published maps and institutional affiliations.



Copyright: © 2021 by the authors. Licensee MDPI, Basel, Switzerland. This article is an open access article distributed under the terms and conditions of the Creative Commons Attribution (CC BY) license (<https://creativecommons.org/licenses/by/4.0/>).

Abstract: The structural, physical–chemical, and micromechanical characteristics of Al_{0.6}Ti_{0.4}N coatings deposited by different physical vapor deposition (PVD) methods, such as cathodic arc deposition (CAD), as well as advanced HiPIMS techniques were investigated in terms of their cutting performance during the machining of an Inconel 718 alloy. XRD studies had revealed that the HiPIMS coating featured lower residual stresses and more fine-grained structure. Electrochemical characterization with the potentiostat-impedance method shows that the HiPIMS coating has a significantly lower porosity than CAD. SEM and AFM studies of the surface morphology demonstrate that the HiPIMS coating has a smoother surface and an absence of droplet phases, in contrast with CAD. XRD, combined with FIB/TEM studies, shows a difference in the crystal structure of both coatings. The micromechanical characteristics of each coating, such as hardness, elastic modulus, fracture toughness, and adhesion to the substrate, were evaluated. The HiPIMS coating was found to possess a more beneficial combination of micromechanical properties compared to CAD. The beneficial characteristics of the HiPIMS coating alleviated the damage of the coated layer under operation. Combined with grain size refinement, this results in the improved adaptive performance of the HiPIMS coating through the formation of a greater amount of thermal barrier sapphire tribofilms on the friction surface. All of these characteristics contribute to the reduction of flank and crater wear intensity, as well as notching, leading to an improvement of the HiPIMS coating's tool life.

Keywords: PVD coatings; cutting tool life; structure; porosity; micro-mechanical characteristics

1. Introduction

Nickel-based superalloys, such as Inconel 718, have been widely used in aerospace, gas turbines, and nuclear industries due to their ability to retain thermal stability and high strength at elevated operating temperatures [1,2]. One of the major difficulties of Inconel 718 machining is its tendency to work harden at elevated temperatures. The hardness of this material increases at temperatures of up to 650 °C [3]. The presence of a certain amount of hard carbide particles (such as TiC, NbC, and others) at the grain boundaries can result in intensive shock loads under operation, which can lead to abrasive wear at the

flank surface of the tool, as well as chipping of the cutting tool edges [4]. The poor thermal conductivity of Inconel leads to the generation of very high temperatures (up to 1000 °C) on the rake surface of the cutting tool [5]. All of these processes also contribute to intensive notching [6]. The other tool wear mechanisms are attrition wear at the rake surface that causes crater wear combined with buildup edge (BUE) formation [4]. To prevent rapid tool failure, the machining of this material has to be conducted at low cutting speeds. The ensuing brief life of the tool results in high machining costs.

Numerous efforts have been made to increase the productivity of the machining process, including optimization of the cutting parameters, first of all cutting speed [7–9], development of novel coolants and lubricants, as well as methods of their supply into the cutting zone [10,11], and, most importantly, surface engineering of the cutting tool [12,13]. The deposition of the coatings on the cemented carbide tool substrate is one of the most commonly used ways of significantly enhancing the tool performance. Coatings promote beneficial heat redistribution and metal flow at the tool/chip interface, improving the wear resistance of the cutting tool.

A thin film hard coating can be applied using the physical vapor deposition (PVD) method. The most commonly used PVD coatings in industry are typically synthesized by the cathodic arc (CAD) method. Another investigated method is HiPIMS (high power impulse magnetron sputtering). Both methods belong to the ionized-PVD category, and have high deposition and plasma ionization rate (current densities in the order of 10^{12} A m⁻²), as well as improved mechanical properties [14]. High power impulse magnetron sputtering (HiPIMS) is a significant improvement in magnetron sputtering techniques. This method is capable of achieving extremely dense plasma at a high ionization rate (pulsed peak ion current densities in the order of $\sim 10^{17}$ – 10^{19} A m⁻² [15,16]).

The TiAlN family of coatings, particularly those with Al content above 50%, are the most widely used for various machining applications [17]. AlTiN coatings provide a more beneficial combination of high thermal/oxidation stability and mechanical properties compared to the previous generation of TiN coatings [15,17]. Aluminum in these coatings quickly diffuses to the friction surface through the grain boundaries and crystal lattice defects, which results in the rapid formation of an Al₂O₃-based surface protective tribo-oxide layer due to the interaction with oxygen from the external environment (air) [18]. The high chemical and thermal stability of the alumina tribo-layers enhance the oxidation resistance and significantly reduce the thermal conductivity of the coating layer. This results in a strong decrease of interdiffusion at the tool/chip interface [19]. A major part of the friction-generated heat is, therefore, transferred into the workpiece instead of the tool during cutting.

Literature has demonstrated that, during the machining of Inconel 718, plastic deformation of the coating layer takes place on both the rake and flank surfaces of the cutting tool [20]. Moreover, the adhesion of workpiece material (Inconel 718) proceeds mostly through mechanical interaction instead of chemical interaction at the tool/workpiece contact area. Under the heavy loads typical of Inconel machining, fracture of the coating layer occurs in the vicinity of surface defects (such as droplets) due to their interaction with the workpiece material [21]. The overall effectiveness of different coatings strongly depends on the extent of operational damage. Fewer defects can reduce the damage of the coated layer, increasing cutting tool life [22–24].

Therefore, the mechanical properties of the coatings, such as hardness, elastic modulus, as well as the ratios thereof (H/E , H^3/E^2), in addition to adhesion to the substrate are of critical importance. Another equally significant characteristic is fracture toughness. A higher toughness helps sustain heavy loads under operation and resist the intermittent shocks during the cutting process [5,12]. The number of macro-defects (such as droplets) present within the coating layer also affects its toughness [12].

This work provides a comprehensive comparative characterization of the structure and properties of AlTiN monolayer coatings deposited by Cathodic Arc (CAD) and by

HiPIMS PVD techniques on carbide cutting tool substrates in relation to their cutting performance during the finish turning of an Inconel 718 aerospace alloy.

2. Materials and Methods

Two $Ti_{0.4}Al_{0.6}N$ monolayer coatings were deposited using $Ti_{0.4}Al_{0.6}$ targets fabricated by a powdered metallurgical process. Mirror polished cemented carbide WC–Co substrates (SPG 422, SPGN12 03 08) were selected for coating characterization, and Kennametal K 313 inserts (CNGG432FS) were chosen for the cutting tool life studies performed on a CNC lathe.

The HIPIMS coating was deposited by an industrial INNOVA Balzers PVD system equipped with a Huettinger TruPlasma Highpulse generator. The target size was 780 cm². A Ti40Al60 (at.%) powder metallurgical target was used. Before deposition, the substrate was heated at 450 °C for 30 min, and etched for 30 min through an Ar discharge with a substrate bias of –170 V. The HIPIMS generator operated at a pulse length of 200 μs, peak currents of 460–600 A, repetition frequency of 400 Hz, and average power of 15 kW. N₂ process pressure was around 1 Pa. The applied bias voltage ranged between –25 V and –130 V.

The CAD coating was deposited by an industrial unit equipped with four circular-shaped evaporators (Kennametal, Frankfurt am Main, Germany). Each evaporator used both a permanent magnet and an adjustable electromagnetic coil to steer the arc. The confinement rings positioned above the cathode had a patented design to stabilize the cubic phase at higher magnetic field intensities. The magnetic field strength was determined to be 100 A/cm at the cathode surface (center) without an applied current. The coil current was set to be either zero (“mag off”) or close to 1 A (“mag on”). The powder metallurgical targets with a diameter of 120 mm and with the same composition were used to deposit the monolayer coating. The chamber temperature was maintained at 500 °C throughout the deposition and the samples were rotated three times. The nitrogen flow rate was controlled to maintain a pressure of 3.5 Pa. The substrate bias voltage was set to –60 V. The cathode current was 200 A. The deposition time was set to 180 min to achieve a coating thickness of around 4 μm.

An XRD X-ray Diffraction System from Proto Manufacturing Limited (LaSalle, ON, Canada) with Cu K α (1.544 Å) radiation was used to determine the crystal structure and preferred orientation of the studied coatings. Residual stresses were measured via a sin² ψ technique with an LXRD Stress Analyzer from Proto Manufacturing. These measurements were performed with a 1.0 mm round aperture in (200) planes identified at 2 θ angles of 80°. A Gaussian function was used to fit the diffraction peaks.

XRD studies of the analyzed coatings were also carried out to identify the formed phases and evaluate the residual stress values using a Siemens D500 diffractometer with a Cu K α tube in the $\theta/2\theta$ mode. The grain size (g.s.) was determined for the main (200) orientation. The standard reference value of the (200) peak in the TiN FCC B1 type structure was (42.633), as specified in the Joint Committee on Powder Diffraction (JCPDS, 87-0633).

A scanning electron microscope (SEM) (Vega 3-TESCAN, Libušina tř., Brno-Kohoutovice, Czech Republic) was used for the detailed inspection of surface morphology of the studied coatings and chips. The surface morphology of the studied coating was also assessed using an Anton Parr Tosca TM 400 atomic force microscope (AFM) (Graz, Austria). Cross-sectional TEM observation was employed in combination with FIB (focused ion beam) for investigation of the coatings on the cemented carbide WC/Co substrates. Transmission electron microscopy and selected area electron diffraction (SAED) were performed in a JEOL FS2200 microscope (JEOL USA, Inc. 11 Dearborn Road, Peabody, MA, USA) at an acceleration voltage of 200 kV and FEI F30 FEG at 300 keV (for the bright field data).

The thickness of the coating was measured by a ball cratering method. The thicknesses of each coating was around 4 microns. The micromechanical characteristics (hardness and elastic modulus) of the coatings were measured through a nanoindentation test (NHT3, Anton Paar, 4920 Place Olivia, Saint-Laurent, QC, Canada). The load applied by a Vickers

indenter during the tests was 20 mN. A matrix of 8×5 indentations was used to collect the relevant data. The hardness and elastic modulus of the coatings were derived from the average of these indentation values. To evaluate the adhesion of the coatings to the carbide substrate, scratch tests were conducted by a Revetest, Anton Paar scratch tester under increasing load from 0.5 to 100 N (distance 3 mm). A Rockwell diamond indenter with a radius of 200 μm was used. Three parameters were evaluated: Lc1—load of the first crack initiation at the coating/substrate interface; Lc2—load at which initial substrate exposure was observed; Lc3—load at which the coating became completely detached from the substrate. Moreover, the fracture toughness of the coatings was measured by the scratch tester equipped with a Vickers indenter at a constant load of 150 N concentrated on a single point. The ISO 28079 standard [22] was used to calculate the toughness of the coatings. The toughness values were calculated using the ratio of the load to the sum of the total crack lengths at the indentation corners. The images of the imprints were taken with Vega 3 TESCAN SEM. Three repetitions were performed for each coating to obtain the adhesion and fracture toughness measurements.

Cutting tool life was studied under turning conditions. Coated Kennametal K 313 cemented carbide inserts were used for the tool life tests. The cutting experiments were carried out on a Nakamura SC450 turning center (8821 60 Ave, Edmonton Alberta T6E6L9). Cutting data is presented in Table 1.

Table 1. Cutting conditions.

Cutting Operation	Workpiece Material	Speed, m/min	Feed Rate, mm/rev	Depth of Cut, mm
Finish turning	Inconel 718 alloy	60	0.1225	0.25

Cutting tests were performed on an Inconel 718 alloy. The cutting conditions were selected based on recommendations from industry, as well as data published in our previous research [23]. At least three cutting tests were performed for each type of coating under the corresponding operating conditions. The scatter of tool life measurements was approximately 5%.

Electrochemical characterization was performed using a potentiostat-impedance analyzer PARSTAT 2273 (Ametek, Oak Ridge, TN, USA) in a 3% NaCl aqueous solution with a 3-electrode corrosion cell containing a working electrode (uncoated or coated substrate), a counter-electrode (Pt mesh), and a reference electrode (SCE, saturated calomel electrode). The results of potentiodynamic studies (1 mV s^{-1} rate) were presented in Tafel plots. Electrochemical impedance spectroscopy (EIS) data were obtained using an alternating current (AC) in the frequency range of 0.01 Hz–10 kHz and voltage amplitude of 5 mV. The EIS data was presented in Bode plots. The porosity values were evaluated based on the results obtained. The immersion time for EIS measurements was 2 h. Cross-sectional TEM observation was employed in combination with FIB (focused ion beam) to investigate the coatings on the cemented carbide WC/Co substrates. Transmission electron microscopy and selected area electron diffraction (SAED) were performed in a JEOL FS2200 microscope and FEI F30 FEG at 300 keV (for the Bright Field data).

The structural and phase transformation at the cutting tool/workpiece interface, as well as the chemical nature of the tribo-films formed, were determined by X-ray photoelectron spectroscopy (XPS) on a Physical Electronics (PHI) Quantera II (Physical Electronics Inc., Chanhassen, MN, USA), equipped with a hemispherical energy analyzer and an Al anode source for X-ray generation and a quartz crystal monochromator for focusing the generated X-rays. A monochromatic Al K-X-ray (1486.7 eV) source was operated at 50 W–15 kV. The system base pressure was as low as 1.0_0_9 Torr, with an operating pressure that did not exceed 2.0_10_8 Torr. Before any spectra were collected from the samples, the samples were sputter-cleaned for four minutes using a 4 kV Ar⁺ beam. A pass energy of 280 eV was used to obtain all survey spectra, while a pass energy of 69 eV was used to collect all high-resolution data. All spectra were obtained at a 45_ take-off

angle and utilized a dual beam charge compensation system to ensure the neutralization of all samples. The instrument was calibrated using a freshly cleaned Ag reference foil, where the Ag 3d5/2 peak was set to 368 eV. All data analyses were performed using PHI Multipak version 9.4.0.7 software. Spots for the high-resolution (HR) analysis were selected based on careful preliminary investigation of general photoelectron spectra of the worn surface close to the buildup edge area.

3. Results

The surface morphology of the studied coating was evaluated through SEM/EDS and AFM studies (Figure 1).

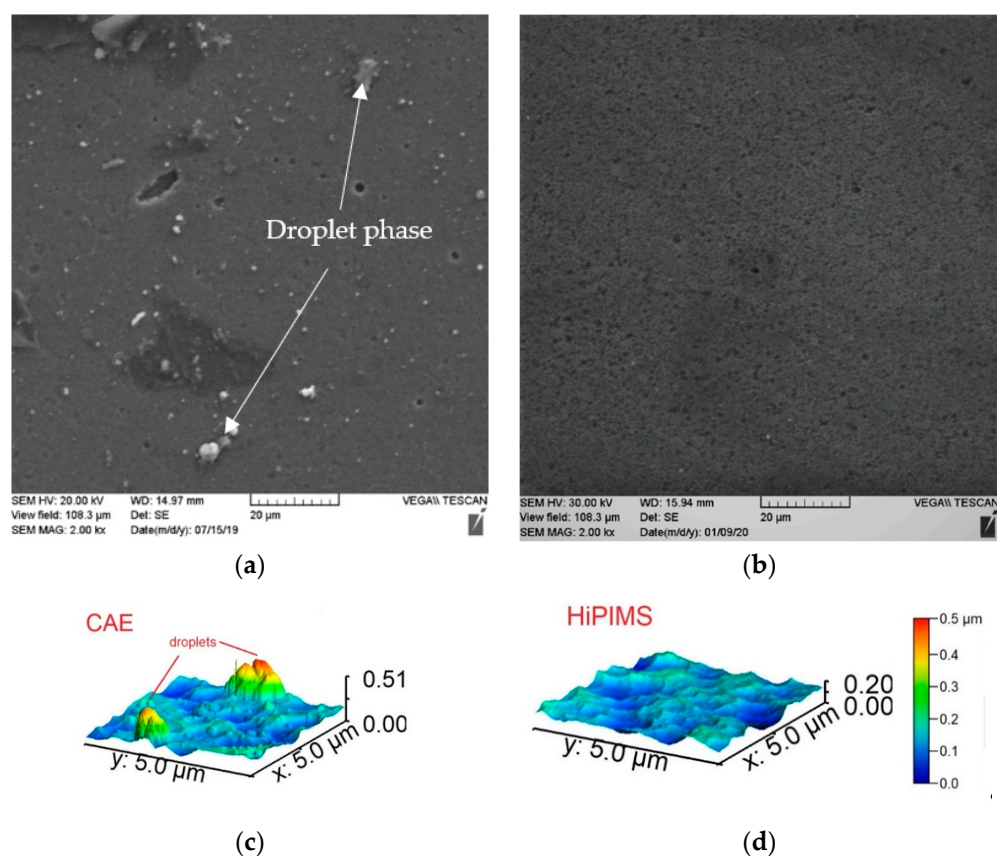


Figure 1. SEM/AFM data on the surface morphology: (a) CAD; (b) HiPIMS coatings: SEM data; (c) CAD; (d) HiPIMS: AFM data.

SEM and AFM surface morphology data show that the coating deposited by HiPIMS possessed a smoother surface and lower porosity compared with that of CAD. Droplet phases were also present only on the surface of the CAD coating (Figure 1a).

Electrochemical evaluation of the studied coatings was performed to obtain numerical data on the porosity of the compared coatings. Figure 2 shows Tafel plots for uncoated and coated substrates. The coated samples exhibit reduced anodic current, which is an indication of corrosion protection being provided to the substrates by the coating.

The protective properties of the coatings have also been studied using the EIS method. Figure 3 shows Bode plots for uncoated and coated substrates. EIS studies (Figure 3) showed increased impedance $|Z|$ in the coated samples, which confirmed that the coatings acted as diffusion barriers for electrolyte ions.

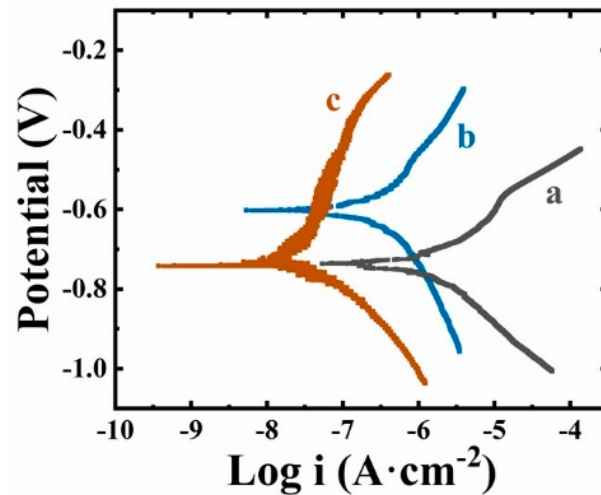


Figure 2. Tafel plots for (a) uncoated and coated substrates, (b) CAD sample, and (c) HiPIMS sample.

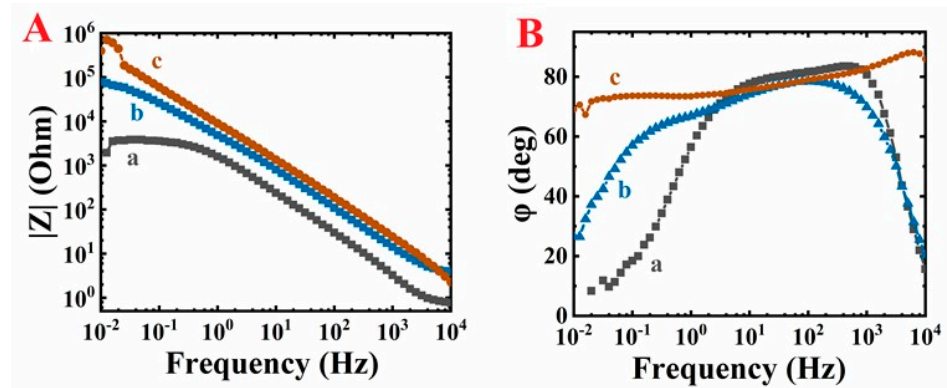


Figure 3. EIS Bode plots of impedance $|Z|$ (A) versus frequency, (B) phase angle versus frequency (B) for (a) uncoated and coated substrates, (b) CAD sample, and (c) HiPIMS sample.

The film porosity (F) was analyzed by a method described in the literature [25,26] using the following equation:

$$F = \frac{R_{pm}}{R_p} \times 10^{-|\Delta E/\beta|} \quad (1)$$

where ΔE represents the corrosion potential difference of the uncoated and coated substrates, β and R_{pm} are the respective anodic Tafel slope and the polarization AC resistance of the uncoated substrate, and R_p represents the polarization AC resistance of the coated substrate. The analysis of the EIS data was performed using the equivalent circuit proposed in [23], which enabled the measurement of R_{pm} and R_p . The film porosity was found to be 0.58% in b (Arc) and 0.12% in c (HiPIMS), see Table 2 below. The measurements allowed for the analysis of pre-existing film porosity [25,26].

Table 2. Porosity values of the studied coatings.

Porosity Values, %	
Arc	0.58
HiPIMS	0.12

It could be concluded that the quantitative porosity data obtained by the polarization method correspond to the initial qualitative SEM data of surface morphology (Figure 1).

The results of the XRD phase analysis are presented in Figure 4. Both coatings show crystalline fcc (B1) structure.

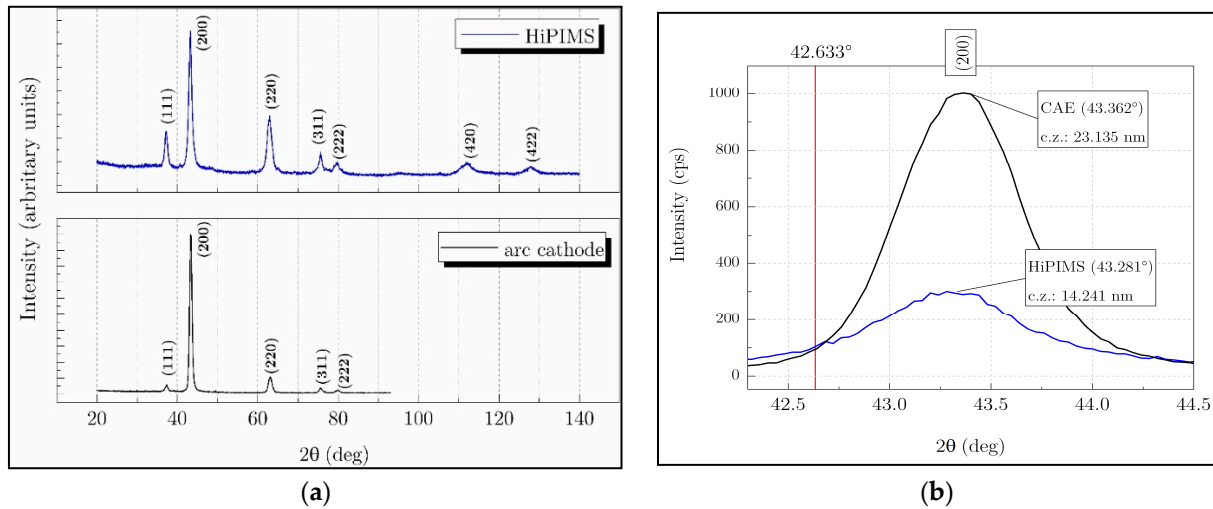


Figure 4. XRD data of the coatings studied: (a) phase composition; (b) full width at half maximum (FWHM) data.

They show that the CAD sample is strongly (200) oriented and the HiPIMS coating is more randomly oriented (Figure 4a). However, the HiPIMS coating still has a significantly preferred orientation. Peak width indicates the fine grain of the HiPIMS sample. This value is an indication of a better-organized structure with lower grain sizes. FWHM data on the studied coatings are presented in Figure 4b. The full width at half maximum (FWHM) value for each coating was derived from XRD data. The grain size (g.s.) was determined for the main (200) orientation (Figure 4a). The average crystalline size of the studied coatings was calculated from the Williamson–Hall relation [27]. It was found that the HiPIMS coating had significantly smaller grain size values of 14, 2 nm in comparison to 23, 1 nm for CAD.

These measurements are in accord with electron diffraction and TEM images.

Figure 5 shows the full view profile for both HiPIMS (a–c) and CAD (d–f) coatings. The electron diffraction presented in Figure 5b shows that the HiPIMS coating has a nanocrystalline structure with a continuous ring pattern characteristic of nanograin size, while the CAD coating shown in Figure 5e features a ring pattern with strong spots associated with a larger grain size (see Figure 4f). The finer grain size in HiPIMS coating affects the adaptive performance of the coatings under operation.

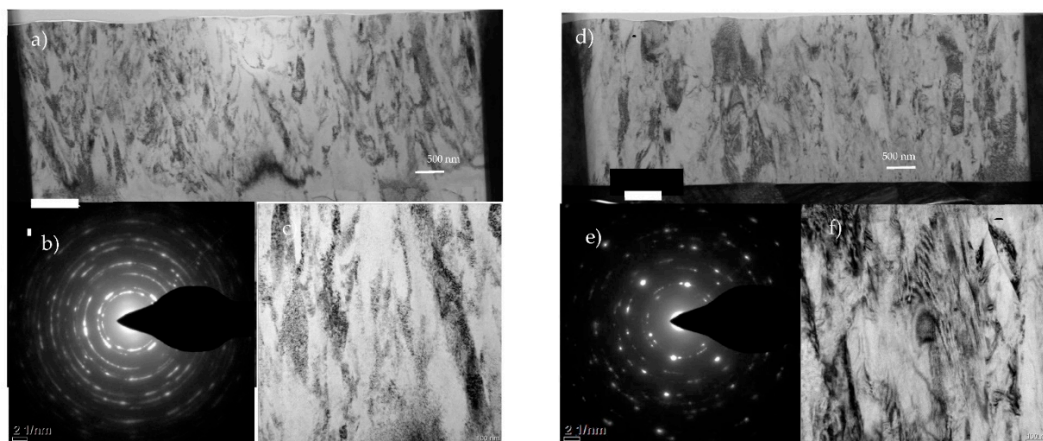


Figure 5. TEM images with SAED diffraction patterns of AlTiN (a–c) HiPIMS and (d–f) CAD coatings.

Micromechanical characteristics of the studied coatings are presented in Table 3.

Table 3. Micromechanical characteristics of the studied coatings.

Coating	Hardness, GPa	Elastic Modulus, GPa	H/E	H ³ /E ²	Lc ₁ , N	Lc ₂ , N	Lc ₃ , N	Palmquist Fracture Toughness	Residual Stresses, GPa
Arc	37.4 ± 2.4	610 ± 23	0.061	0.368	50.6 ± 1	52 ± 1	53.9 ± 1	0.213 ± 0.012	−1.88 ± 0.31
HiPIMS	42.9 ± 3.2	615 ± 25	0.069	0.418	63.9 ± 1	72.1 ± 1	73.9 ± 1	0.277 ± 0.013	−1.615 ± 0.27

Micromechanical data show that the HiPIMS coating features the following beneficial properties: higher hardness, better loading support (H³/E²), strongly increased adhesion (Table 3, Figure 6), lower residual stresses, as well as improved fracture toughness (Table 3, Figure 7) [28–32]. The last characteristic is directly related the lower porosity values of the coating (Table 2).

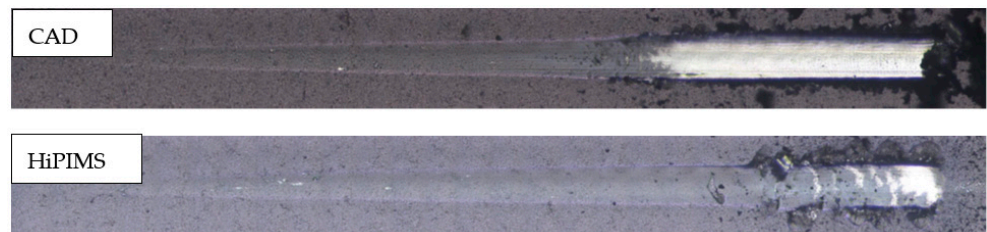


Figure 6. Adhesion of the studied coatings to the carbide substrate.

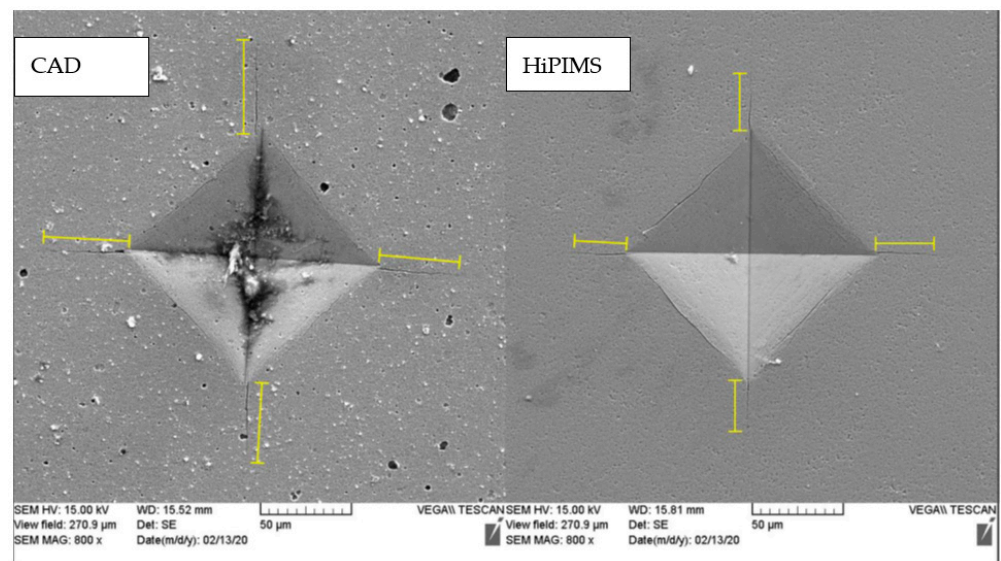


Figure 7. Fracture toughness of the studied coatings.

This combination of properties enhances resistance to abrasion and impact loading, due to the presence of carbide particles within the structure of the machined material and the unstable process of buildup edge (BUE) formation typical for Inconel 718 machining.

The coatings' wear performance was characterized by flank wear vs. length of cut data (Figure 8), which demonstrated that the HiPIMS coating had outperformed CAD by around 60%.

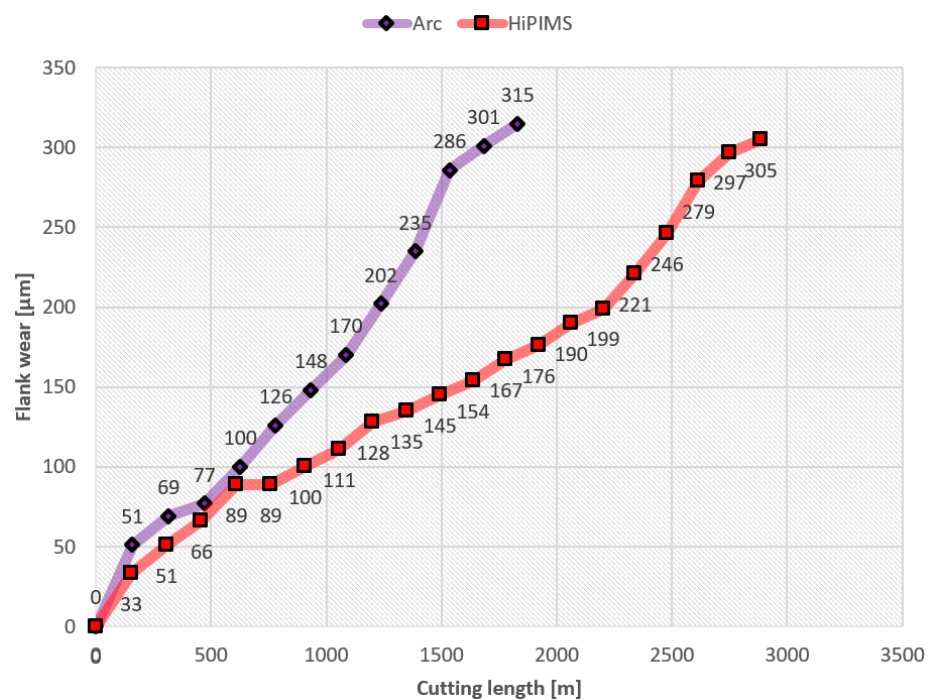


Figure 8. Flank wear vs. length of cut data for the coatings studied.

Wear patterns were evaluated through 3D optical microscopy imaging (Figure 9). The presented data show that catastrophic failure of the CAD coating occurs after 1200 m (Figure 8), due to a combination of severe crater wear and BUE formation. At the same time, the flank surface undergoes intensive notch wear and abrasion. This results in substrate exposure on the flank surface. All of these processes are significantly diminished on the tool with an HiPIMS coating.

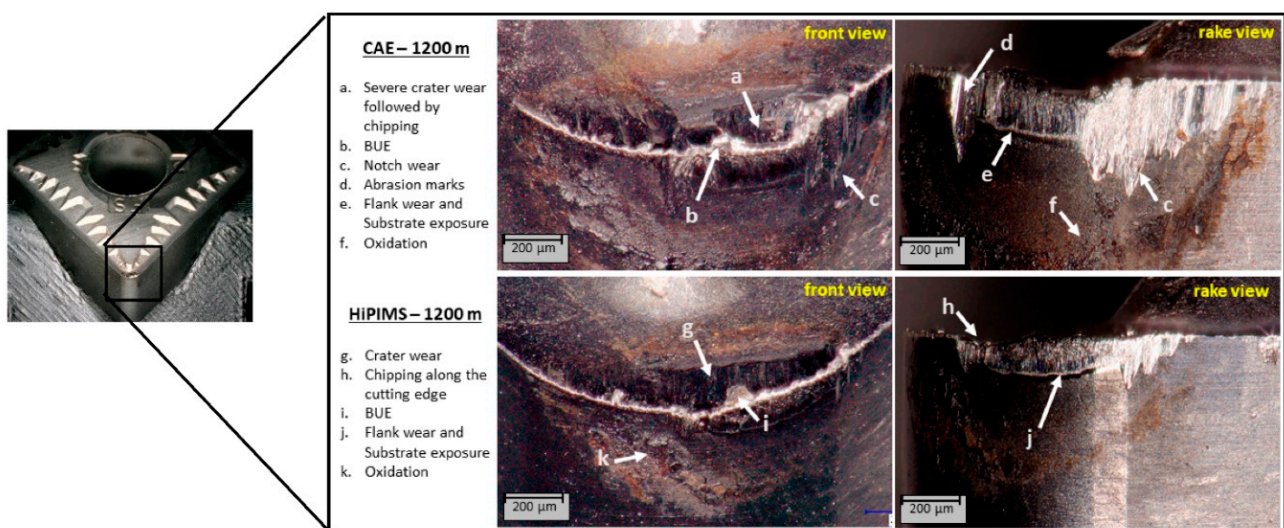


Figure 9. 3D optical images of the worn tools with the studied coatings after length of cut of 1200 m.

XPS studies of the worn tool surface were performed (Figure 10) and the XPS data presented show that the worn HiPIMS-coated tool had experienced the formation of a greater amount of sapphire tribo-films compared to the CAD-coated tool (89.9% vs. 76.9%) [33].

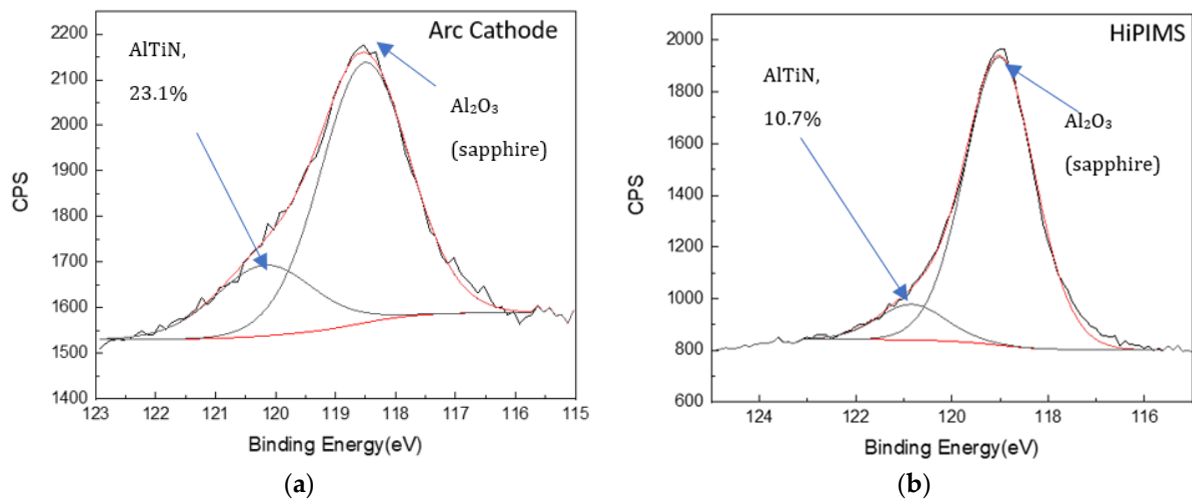


Figure 10. XPS data on the tribo-films formation on the friction surface of the cutting tool with: (a) CAD; (b) HiPIMS AlTiN coating.

This is one of the primary reasons for its superior tool life compared with CAD, since sapphire acts as a thermal barrier, which protects the friction surface under operation. The increase in the amount of thermal barrier tribo-films that form on the friction surface is a result of the acceleration of aluminum diffusivity during tribo-oxidation. The structural characteristics of the HiPIMS coating (Figures 4 and 5) directly affect this phenomenon. Reduced surface damage, in combination with the smaller grain size of the HiPIMS coating (Figure 5b), facilitates the formation of protective aluminum-based tribo-oxide films [19,20] and improves the adaptive performance of the surface engineered layer [33].

The tribological performance of the coatings was evaluated through the study of chip characteristics. Undersurface morphology (Figure 11a) reveals several sticking points on the undersurface of chips generated by the CAD-coated tool. In contrast, the chips formed by the tool with an HiPIMS coating exhibit a smooth undersurface (Figure 11b). This is an indication of superior tribological conditions at the chip/tool interface.

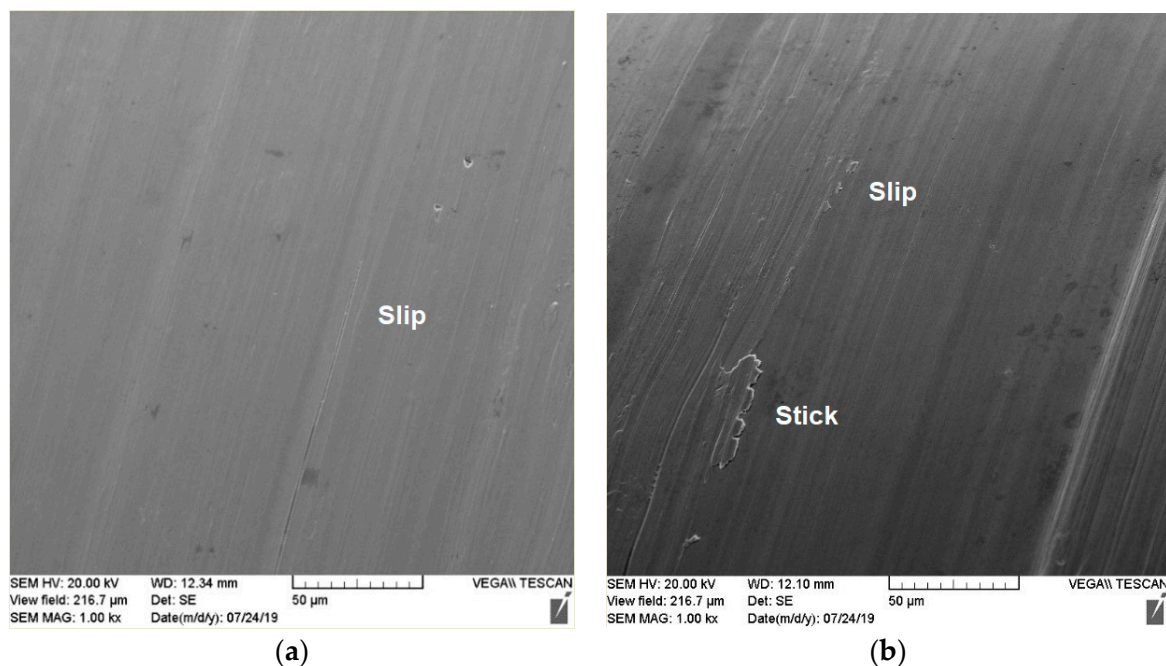


Figure 11. Chips undersurface produced by cutting tool with: (a) CAD and (b) HiPIMS coating.

Figure 12 shows SEM images of the upsurface of the chips. The formation of large serrations is a consequence of the high chip strain caused by the intense cutting forces. The HiPIMS chips exhibited smaller serrations, which signifies a reduction in the forces generated during cutting, an indication of superior tribological performance.

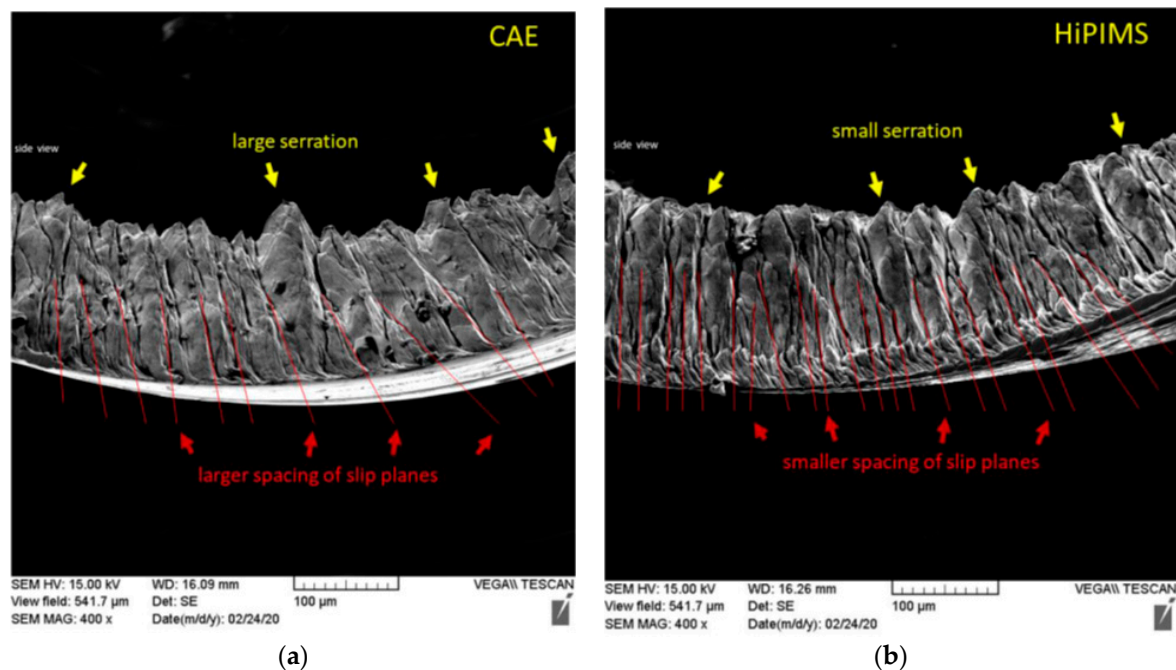


Figure 12. Chips upsurface produced by cutting tool with: (a) CAD and (b) HiPIMS coating.

4. Conclusions

The cutting performance of $Al_{0.6}Ti_{0.4}N$ coatings deposited on carbide tool substrates by two different PVD methods, cathodic arc and advanced HiPIMS techniques, underwent a comprehensive characterization study during the machining of an Inconel alloy. The HiPIMS coating was found to possess a significantly lower porosity. The hardness and H^3/E^2 ratio of HiPIMS was greater than that of CAD, which provides critically important load support for the heavy load operating conditions of Inconel machining. At the same time, adhesion of the HiPIMS coating to the carbide substrate was also noticeably higher than in CAD. Combined with fracture toughness, which is directly related to the porosity of the coating, these characteristics impede the major tool wear mechanisms, thereby leading to the improvement of tool life. The smaller grain size of the HiPIMS coating accelerates the diffusion of aluminum during tribo-oxidation. Combined with the reduction of operational damage, this affects the adaptive performance of the HiPIMS coating due to the formation of a greater amount of thermal barrier sapphire tribo-films on the friction surface.

Each of these parameters contributes to the reduction of the intensity of the major wear processes, resulting in an overall improvement of the HiPIMS coating's tool life by around 60%. It should be noted that this combination of characteristics is highly application specific.

Author Contributions: Conceptualization, G.F.-R.; methodology, L.W.R., M.H.A., K.Y., and I.Z.; investigation, L.W.R., M.H.A., K.Y., and Q.Z.; writing—original draft preparation, L.W.R.; writing—review and editing, G.F.-R., M.H.A., and I.Z.; supervision, funding acquisition, S.C.V. All authors have read and agreed to the published version of the manuscript.

Funding: This research was funded by Natural Sciences and Engineering Research Council of Canada NSERC Grant NETGP 479639-15.

Institutional Review Board Statement: Not applicable.

Informed Consent Statement: Not applicable.

Data Availability Statement: All data presented in current manuscript. For further query communicate with corresponding author.

Acknowledgments: The authors also acknowledge the McMaster Manufacturing Research Institute (MMRI) for the use of its facilities. Critical proofreading of the manuscript by Michael Dosbaev is acknowledged.

Conflicts of Interest: The authors declare no conflict of interest.

References

1. Pollock, T.M.; Tin, S. 102 Nickel-based superalloys for advanced turbine engines chemistry, microstructure, and properties. *J. Propuls. Power* **2006**, *22*, 361–374. [[CrossRef](#)]
2. Schafrik, R.; Sprague, R. Gas turbine materials. *Adv. Mater. Process.* **2004**, *5*, 29–34.
3. Shokrani, A.; Dhokia, V.; Newman, S. Environmentally conscious machining of difficult-to-machine materials with regard to cutting fluids. *Int. J. Mach. Tools Manuf.* **2012**, *57*, 83–101. [[CrossRef](#)]
4. Sharman, A.; Dewes, R.C.; Aspinwall, D.K. Tool life when high speed ball nose end milling Inconel 718TM. *J. Mater. Process. Technol.* **2001**, *118*, 29–35. [[CrossRef](#)]
5. Sun, S.; Brandt, M.; Dargusch, M.S. Thermally enhanced machining of hard-to-machine materials A review. *Int. J. Mach. Tools Manuf.* **2010**, *50*, 663–680. [[CrossRef](#)]
6. Cantero, J.L.; Díaz-Álvarez, J.; Miguélez, M.H.; Marín, N.C. Analysis of tool wear patterns in finishing turning of Inconel 718. *Wear* **2013**, *297*, 885–894. [[CrossRef](#)]
7. Asha, P.; Rao, C.P.; Kiran, R.; Kumar, D.R. Effect of machining parameters on cutting tool temperature and tool life while turning EN24 and hchr grade alloy steel. *Mater. Today Proc.* **2018**, *5*, 11819–11826. [[CrossRef](#)]
8. Pathak, A.; Warghane, R.; Deokar, S. Optimization of cutting parameters in dry turning of AISI A2 tool steel using carbide tool by taguchi based fuzzy logics. *Mater. Today Proc.* **2018**, *5*, 5082–5090. [[CrossRef](#)]
9. Paturi, U.M.R.; Devarasetti, H.; Narala, S.K.R. Application of regression and artificial neural network analysis in modelling of surface roughness in hard turning of AISI 52100 steel. *Mater. Today Proc.* **2018**, *5*, 4766–4777. [[CrossRef](#)]
10. Rahim, E.A.; Sasahara, H. An analysis of surface integrity when drilling inconel 718 using palm oil and synthetic ester under MQL condition. *Mach. Sci. Technol.* **2011**, *15*, 76–90. [[CrossRef](#)]
11. Bushlya, V.; Lenrick, F.; Ståhl, J.E.; M'Saoubi, R. Influence of oxygen on the tool wear in machining. *CIRP Ann.* **2018**, *67*, 79–82. [[CrossRef](#)]
12. Li, G.; Li, L.; Han, M.; Luo, S.; Jin, J.; Wang, L.; Gu, J.; Miao, H. The performance of TiAlSiN coated cemented carbide tools enhanced by inserting Ti interlayers. *Metals* **2019**, *9*, 918. [[CrossRef](#)]
13. Hosokawa, A.; Hoshino, G.; Koyano, T.; Ueda, T. Cutting characteristics of PVD-coated tools deposited by filtered arc deposition (FAD) method. *CIRP Ann.* **2018**, *67*, 83–86. [[CrossRef](#)]
14. Olbrich, W.; Fessmann, J.; Kampschulte, G.; Ebberink, J. Improved control of TiN coating properties using cathodic arc evaporation with a pulsed bias. *Surf. Coat. Technol.* **1991**, *49*, 258–262. [[CrossRef](#)]
15. Luo, Q.; Yang, S.; Cooke, K. Hybrid HIPIMS and DC magnetron sputtering deposition of TiN coatings: Deposition rate, structure and tribological properties. *Surf. Coat. Technol.* **2013**, *236*, 13–21. [[CrossRef](#)]
16. Anders, A. Discharge physics of high power impulse magnetron sputtering. *Surf. Coat. Technol.* **2011**, *205*, S1–S9. [[CrossRef](#)]
17. Leyendecker, T.; Lemmer, O.; Esser, S.; Ebberink, J. The development of the PVD coating TiAlN as a commercial coating for cutting tools. *Surf. Coat. Technol.* **1991**, *48*, 175–178. [[CrossRef](#)]
18. Fox-Rabinovich, G.S.; Yamamoto, K.; Beake, B.D.; Kovalev, A.I.; Aguirre, M.H.; Veldhuis, S.C.; Dosbaeva, G.K.; Wainsteind, D.L.; Biksa, A.; Rashkovskiy, A. Emergent behavior of nano-multilayered coatings during dry high-speed machining of hardened tool steels. *Surf. Coat. Technol.* **2010**, *204*, 3425–3435. [[CrossRef](#)]
19. Endrino, J.; Fox-Rabinovich, G.; Gey, C. Hard AlTiN, AlCrN PVD coatings for machining of austenitic stainless steel. *Surf. Coat. Technol.* **2006**, *200*, 6840–6845. [[CrossRef](#)]
20. Koseki, S.; Inoue, K.; Usuki, H. Damage of physical vapor deposition coatings of cutting tools during alloy 718 turning. *Precis. Eng.* **2016**, *44*, 41–54. [[CrossRef](#)]
21. Akhtar, W.; Sun, J.; Sun, P.; Chen, W.; Saleem, Z. Tool wear mechanisms in the machining of Nickel based super-alloys: A review. *Front. Mech. Eng.* **2014**, *9*, 106–119. [[CrossRef](#)]
22. *The ISO 28079 Standard, Hardmetals, Palmquist Fracture Toughness Test, Powder Metallurgy, Subcommittee SC 4*; ISO: Geneva, Switzerland, 2009.
23. Capasso, S.; Paiva, J.; Junior, E.L.; Settineri, L.; Yamamoto, K.; Amorim, F.; Torres, R.; Covelli, D.; Fox-Rabinovich, G.; Veldhuis, S. A novel method of assessing and predicting coated cutting tool wear during Inconel DA 718 turning. *Wear* **2019**, *432–433*, 202949. [[CrossRef](#)]
24. Liu, C.; Bi, Q.; Leyland, A. Matthews. *Corros. Sci.* **2003**, *45*, 1257–1273. [[CrossRef](#)]

25. Tato, W.; Landolt, D. Electrochemical determination of the porosity of single and duplex PVD coatings of titanium and titanium nitride on brass. *J. Electrochem. Soc.* **1998**, *145*, 4173–4181. [[CrossRef](#)]
26. Mote, V.D.; Purushotham, Y.; Dole, B.N. Williamson-Hall analysis in estimation of lattice strain in nanometer-sized ZnO particles. *J. Theor. Appl. Phys.* **2012**, *6*, 2–9. [[CrossRef](#)]
27. Malzbender, J.; de With, G.; den Toonder, J.M.J. Elastic modulus, indentation pressure and fracture toughness of hybridcoatings on glass. *Thin Solid Films* **2000**, *366*, 139–149. [[CrossRef](#)]
28. Wang, X.; Wang, C.; Atkinson, A. Interface fracture toughness in thermal barrier coatings bycross-sectional indentation. *Acta Mater.* **2012**, *60*, 6152–6163. [[CrossRef](#)]
29. Donohue, E.M.; Philips, N.R.; Begley, M.R.; Levi, C.G. Thermal barrier coating toughness: Measurement and identification of a bridging mechanism enabled by segmented microstructure. *Mater. Sci. Eng. A* **2013**, *564*, 324–330. [[CrossRef](#)]
30. Shukla, K.; Purandare, Y.P.; Khan, I.; Ehiasarian, A.P.; Hovsepian, P.E.H. Effect of nitriding voltage on the impact load fatigue and fracture toughness behaviour of CoCrMo alloy nitrided utilising a HIPIMS discharge. *Surf. Coat. Technol.* **2020**, *400*, 126227. [[CrossRef](#)]
31. Byakova, A.V.; Gorbach, V.G. Fracture toughness and evaluation of coating strength with an initial residual stress field. *Strength Mater.* **1994**, *26*, 40–48. [[CrossRef](#)]
32. Fox-Rabinovich, G.; Kovalev, A.; Gershman, I.; Wainstein, D.; Aguirre, M.H.; Covelli, D.; Paiva, J.; Yamamoto, K.; Veldhuis, S. Complex behavior of nano-scale tribo-ceramic films in adaptive PVD coatings under extreme tribological conditions. *Entropy* **2018**, *20*, 989. [[CrossRef](#)] [[PubMed](#)]
33. Fox-Rabinovich, G.S.; Gershman, I.S.; Yamamoto, K.; Aguirre, M.H.; Covelli, D.; Arif, T.; Aramesh, M.; Shalaby, M.; Veldhuis, S. Surface/interface phenomena in nano-multilayer coating under severing tribological conditions. *Surf. Interface Anal.* **2016**, *49*, 584–593. [[CrossRef](#)]